

IB Physics
Internal Assessment

*Investigating the effect of irradiance on
the internal resistance of photovoltaic cells*

Candidate personal code : gnm174

Date: 13/03/2020

Introduction

Solar power is at the forefront of the fight to sustainably meet the world’s growing energy needs. However, solar must overcome several significant hurdles in order to achieve widescale adoption. Solar cells differ from many other sources of electricity in that they produce energy exclusively when exposed to light, and this energy cannot be stored in the system, instead requiring a direct feed into the local grid or external batteries. Like batteries, solar cells contain an internal ‘series resistance’ that reduces efficiency and can lead to overheating; however, they differ in that this internal resistance is highly illumination- and temperature-dependent. A strong understanding of the internal series resistance mechanisms in a solar panel is therefore critical to efficient power generation, laying the groundwork for technologies ranging from the moonshot DESERTEC to the ubiquitous home solar panel.

Research question

What is the effect of incident irradiance G (in $W \cdot m^{-2}$) on the series resistance R_S (in Ω) of a sample polycrystalline photovoltaic solar cell?

Background research

Photovoltaics

Photovoltaic cells, also known as PV or solar cells, are composed of thin layers of a semi-conductor such as silicon (Figure 1). When the surface of the panel is exposed to electromagnetic radiation with an energy greater than or equal to the semi-conductor’s work function ϕ , electrons are energized and thus dislodged from their atom in the panel base. These high-energy delocalized electrons are then forced through a charged p-n junction to flow out of a panel terminal. They flow around the circuit, dissipating their energy before arriving back at the low-potential area of the circuit, ready to be re-energized [1].

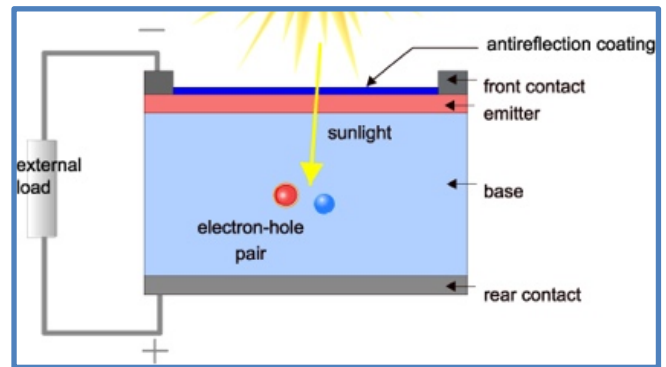


Figure 1. Cross-section of a PV cell [2]

Parasitic resistances

Photovoltaic cells are similar energy sources to normal batteries, but with several key distinctions. Using the single-diode model [3]–[5], photovoltaic cells can be modelled as the combination of a source of current, a diode, an internal (series) resistance R_S , in addition to a ‘shunt resistance’ R_{SH} across the two terminals – as shown in the general equivalent circuit in Figure 2. In conventional battery setups, both the supplied current I (in A) and internal resistance remain constant assuming constant temperature. In photovoltaic cells, by contrast, the supplied current and internal resistance are dependent not only on temperature, but on irradiance as well. These two resistances are responsible for losses in power and are therefore known as ‘parasitic’ resistances. These two parasitic resistances R_S and R_{SH} can be understood as follows:

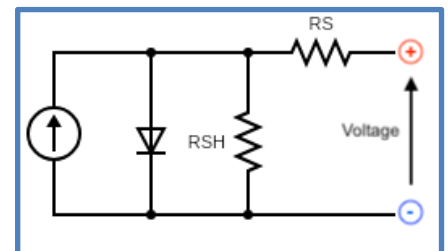


Figure 2. Solar cell equivalent single-diode circuit diagram.

- **Shunt resistance** R_{SH} is a representation of power losses due to the diversion of current in a solar cell, caused by factors such as irregularities in the panel's doped layers, or external pathing on the outside of the cell. At low shunt resistances, this current diversion results in less current flowing across the main measured circuit junction, and hence voltage losses. In an ideal solar cell, shunt resistance value would have a value tending toward infinity, such that none of the current would be short-circuited / diverted from the main potentiometer loop. Cheap low-quality panels--such as the one used in this experiment--are the most likely to be affected by the parasitic effects of low shunt resistances. However, this will not impact our investigation, as the net change in R_{SH} with changing irradiance can be presumed negligible [6].
- **Series resistance** R_S quantifies the losses in series with our EMF source. R_S originates from sites of poor conduction, whether low-quality wires, corroded contacts, or factors intrinsic to the cell design. A large increase in the series resistance would result in a slightly reduced current output and significantly reduced 'fill factor' (FF)—a measure of the maximum obtainable power from a cell.

For an ideal solar cell, the series resistance would be zero such that no energy is unnecessarily dissipated in resistors other than the target load, and thus the ideal target load would be infinite. However, for non-ideal solar cells that have a non-negligible series resistance, a slightly less straightforward relationship exists between R_S and the optimum external load for power dissipation (Maximum Power Point, $R_{L,MPP}$). This can be found using the maximum power transfer theorem, derived as follows [7].

Starting with Ohm's law:

$$V = I \cdot R \rightarrow I = \frac{V}{R} \quad (1)$$

Hence the circuit current can be found as the supplied EMF (V) over the sum of R_L and R_S

$$I = \frac{V}{R_L + R_S} \quad (2)$$

where R_L is the load resistance that can be arbitrarily set using a potentiometer/variable resistor, and R_S is the series resistance. Now, merging eq. 2 with the formula for the power dissipated in a circuit (eq. 3):

$$P = I^2 R \quad (3)$$

$$P_L = \left(\frac{V}{R_L + R_S} \right)^2 R_L \quad (4)$$

The function for P_L in eq. 4 contains only one maximum power output, which can be found by taking the derivative of P_L with respect to R_L , and equating this derivative to zero to find this local maximum at $\frac{dP_L}{dR_L} = 0$:

$$\frac{dP_L}{dR_L} = \frac{(R_L + R_S) \cdot V^2 - 2V^2 R_L}{(R_L + R_S)^3} \quad (5)$$

$$\frac{dP_L}{dR_L} = 0 \rightarrow (R_L + R_S) \cdot V^2 - 2V^2 R_L = 0 \quad (6)$$

$$(R_L + R_S) - 2R_L = 0 \quad (7)$$

$$\therefore R_L = R_S \quad (8)$$

This tells us that the optimum external load R_L for maximizing power output is simply equal to the internal series resistance of the cell, R_S .

This information is extremely useful, because it means that if we were to vary the resistance of a potentiometer connected to a solar cell in a circuit such as the one shown in Figure 2, the resistance that produces optimum output power (the MPP) would also give us the internal series of the cell.

Hypothesis

According to previous researchers, the variation of shunt resistance R_{SH} with irradiance G is negligible for several types of tested panels, including polycrystalline [6], in the range $G \leq 500 \text{ W} \cdot \text{m}^{-2}$. The same will be assumed true here, meaning that the initial R_{SH} may manifest itself as a constant systematic error through the results, but will have no bearing on the G vs. R_S relationship.

Numerous studies have established that the series resistance R_S appears to decrease continuously with irradiation intensity [3][8]. Furthermore, several studies have found an inversely proportional relationship between the irradiance G and series resistance R_S [9][10][11], alluding to a curved downward slope with maximum R_S as $G \rightarrow 0$, and a convergence to $R_S = 0$ with increasing G , as seen in Figure 3. In their 2009 paper N.H. Reich et al. [12] explicitly describe the relationship as a power law, finding that the series resistance exponentially decreased with illumination:

$$R_S = a \cdot G^b \quad (9)$$

where constants a and b were found empirically, with b found to approximate -1 , although these constants were likely specific to the panel used.

Explanations for this effect attribute the decrease in R_S with G to increases in the conductivity of the active layer, allowing for the release of more free delocalized electrons with increasing irradiance.

Based on this literature review, we expect a power relationship between the two variables, but the precise value of the exponents and coefficients cannot be determined analytically and will therefore be found empirically.

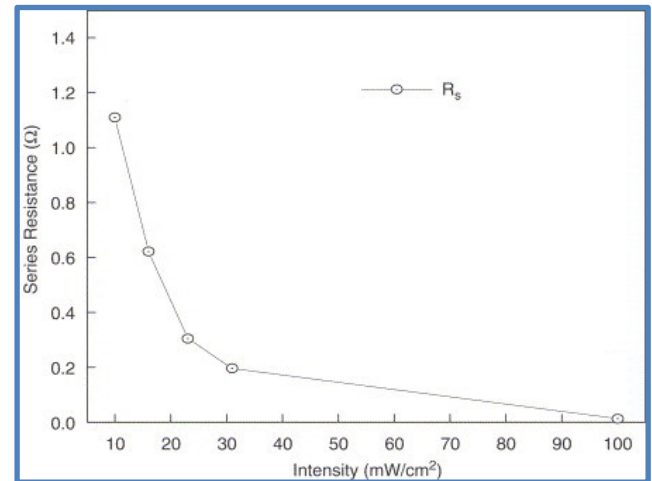


Figure 3. Literature graph of R_S vs. G . [9]

Methodology

Variables

Independent: The mean irradiance intensity G incident on our solar panel, provided by a Leica slide projector, measured using a luxmeter (with values converted to $W \cdot m^{-2}$). This was varied by changing the distance of the projector using a ruler, moved in increments of 5 or 10 cm. Nine distance measurements were conducted, with 5 trials for each. The mean of the intensities recorded throughout the 5 trials were used as the independent variable.

Distance (cm)	32	37	42	47	57	62	72	82	92
Mean Illuminance ($lm \cdot m^{-2}$)	40620	30982	25546	21262	14616	12756	9784	7379	6199
Mean Irradiance G ($W \cdot m^{-2}$)	321	245	202	168	115	101	77	58	49

Dependent: The internal series resistance of the solar panel R_S (in Ω), found graphically using Logger Pro software as the peak of a power-resistance graph at each luminosity increment, generated using measurements with a voltmeter (V) and ammeter (A).

Controlled & Uncontrolled:

Controlled		
Variable	Effect on data	How the variable is controlled
Panel temperature	The panel surface temperature is one of the two external factors that could have an effect on both parasitic resistances (the other being the illuminance), therefore it was imperative to keep temperature constant during the experiment.	During preliminary trials it became apparent that the solar panel received very little heat from the projector. Nowhere in the range of 20-100 cm could any heating effect on the solar panel surface be discerned by touch, even after all 5 trials were taken. As a precaution, the projector was switched off between trials and the range modified to start at 32 cm.
Series resistance outside of solar panel	As explained in the introduction, the internal series resistance describes the sum of all the poor-conductivity sections of the solar cell, including the back/front contacts and wires. For this reason, a change in wires or the circuit could result in a change in the series resistance for reasons other than irradiance.	The apparatus was left undisturbed during the experiment where possible, and strong, insulated connections were created between wires and components.
Irradiance spectrum	Photovoltaic cells work best with certain frequencies of light in the electromagnetic spectrum, with a direct effect on the efficiency and induced photocurrent I_{PH} in the cell.	The irradiance spectrum provided by the projector was kept consistent throughout the trials by using the same halogen bulb throughout. The safety precautions / panel temperature control method, also has the added benefit of preventing spectrum shifts due to the bulb overheating [13] (although the effects of this are arguably negligible).

Uncontrolled		
Air mass	Standard Test Conditions (STC), the industry standard for evaluation and comparison of solar cells, call for various conditions including $1.0 \text{ kW} \cdot \text{m}^{-2}$ irradiation, temperature of 25°C , and air mass coefficient of 1.5. The first two are independent and controlled variables, respectively, while the last is too difficult to control given the resources available.	The air mass and temperature were assumed constant, and the investigation was carried out in a single sitting.

Safety

Risk Assessment

Two sources of risk were identified: the projector heating, and the circuit current/voltage. The projector uses an OSRAM 150W halogen light bulb [14], which poses a low risk of fire as long as projector air vents are left unobstructed and the projector is turned off when not in use. The solar panel circuit was found to conform to class 3 of IEC standard 60950-1—a “SELV (Safety Extra Low Voltage) supply circuit”—meaning that the operator is safe from shocks since peak voltage and current values are well within human safety limits.

Ethical considerations

There were no ethical considerations deemed significant enough to impact the investigation.

Method

Table 3: Apparatus	
Materials	
Leica slide projector (150 W)	Digital luxmeter (± 100 lux)
Polycrystalline solar panel ($7 \times 10 \text{ cm}^2$)	Retort stand + clamp
Digital voltmeter ($\pm 0.005 \text{ V}$)	2x $2\text{k}\Omega$ potentiometers
Digital ammeter ($\pm 0.005 \text{ A}$)	Laptop with Logger Pro software for data logging
1 m ruler ($\pm 0.01 \text{ m}$)	

Setup

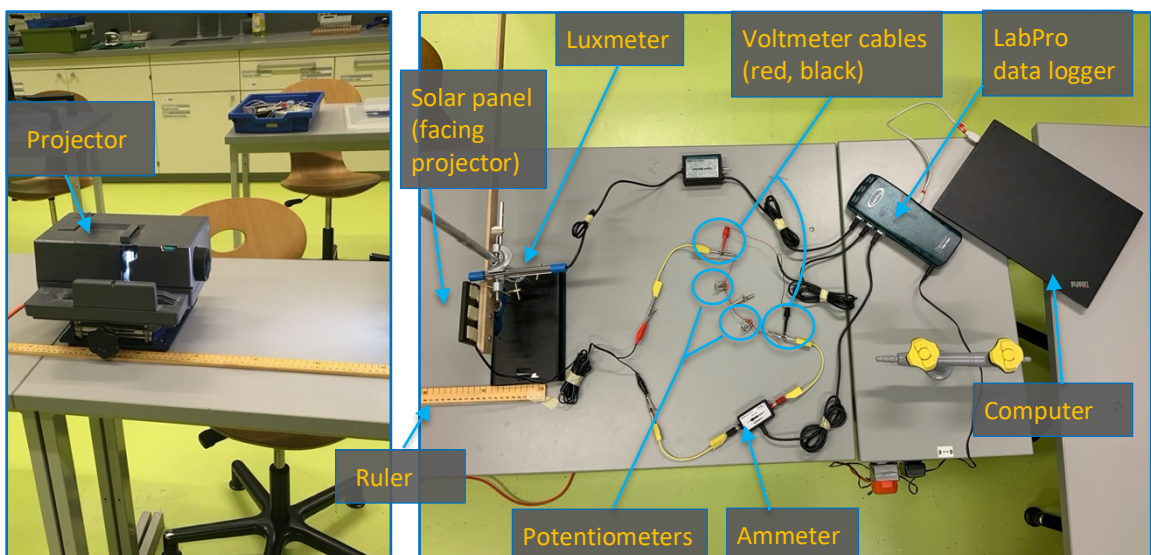


Figure 4. Material setup showing projector, solar panel, and circuit

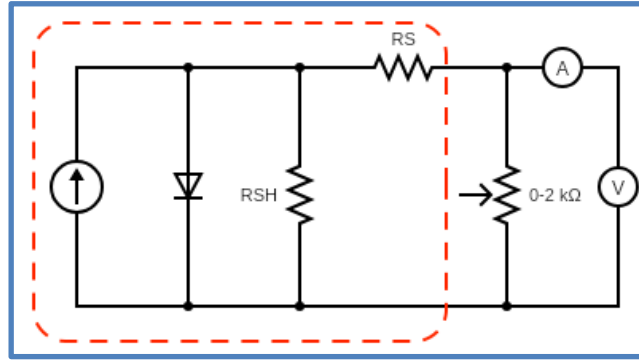


Figure 5. Circuit setup diagram, with PV cell delineated by red box

Pre-experiment

1. Set up the apparatus as shown in Figure 4, with circuitry connected according to Figure 5.
2. Configure Logger Pro or equivalent data collection software to display a graph of current vs. voltage. Add two ‘calculated columns’ to record the power dissipated in the variable resistor and its resistance, using the formulas 2a, 2b, below. Then, the ‘power dissipated’ column should be set to graph against the resistance column.

a. Power dissipated: $P = V \cdot I$

b. Load resistance: $R = \frac{V}{I}$

3. Turn off all light sources other than the projector and darken the lab (as much as possible).

Trial Procedure

4. Reset both 1 kΩ potentiometers to 0 Ω.
5. Turn on the projector and start logging.
6. Very slowly start increasing the resistance with the potentiometers, and gradually increase the speed until the maximum 2 kΩ are reached. The slow start is important because, as became evident during preliminary trials, the beginning of the amperage downturn in the I-V graph (see: Figure 7 on following page) is likely to happen within the first ~100 Ω for high irradiances and ~500 Ω for low-light trials. Note that after preliminary trials, the resistance range will likely need to be re-evaluated and empirically tested depending on the panel size, output, and model to see whether it produces a sufficient portion of the I-V curve to show points of interest (ex. MPP, V_{OC}, I_{SC}).
7. Stop logging and turn off the projector. If the surface of the solar panel has warmed to the touch, the trial data must be deleted, and the trial redone after a 5-minute cooldown.
8. Repeat step 4-7 for each of the 5 trials at each of the 9 distances (32, 37, 42, 47, 57, 62, 72, 82, 92 cm ±1 cm).

Results and data

Data processing

Finding the Maximum Power Point

Using the logic developed for the maximum power transfer theorem in the introduction, the internal resistance of the cell can be found as the external load resistance that would maximize power output. Hence, circuit parameters that maximize the power output for a given trial and illumination can be used to find the MPP using the power dissipated law and load resistance law.

For standard power dissipation optimization problems, such as those for batteries, a custom trendline with parameters shown in eq. 10 can be used. However, a satisfactory formula could not be reliably adapted for fitting the PV cell data, due to the additional variables associated with solar cells (see: Figure 6).

$$P = R_S \cdot \frac{I^2}{(R_S + R_L)^2} \tag{10}$$

For this reason, a power vs. voltage graph was used for finding the MPP instead.

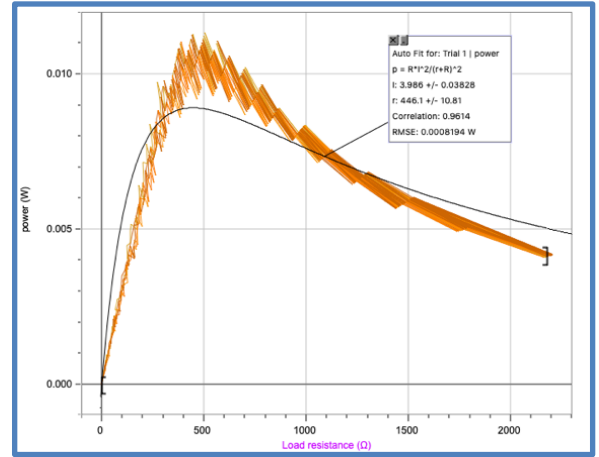


Figure 6. Unsatisfactory trendline for power-resistance plot at 820 cm ($G=58 \text{ W} \cdot \text{m}^2$)

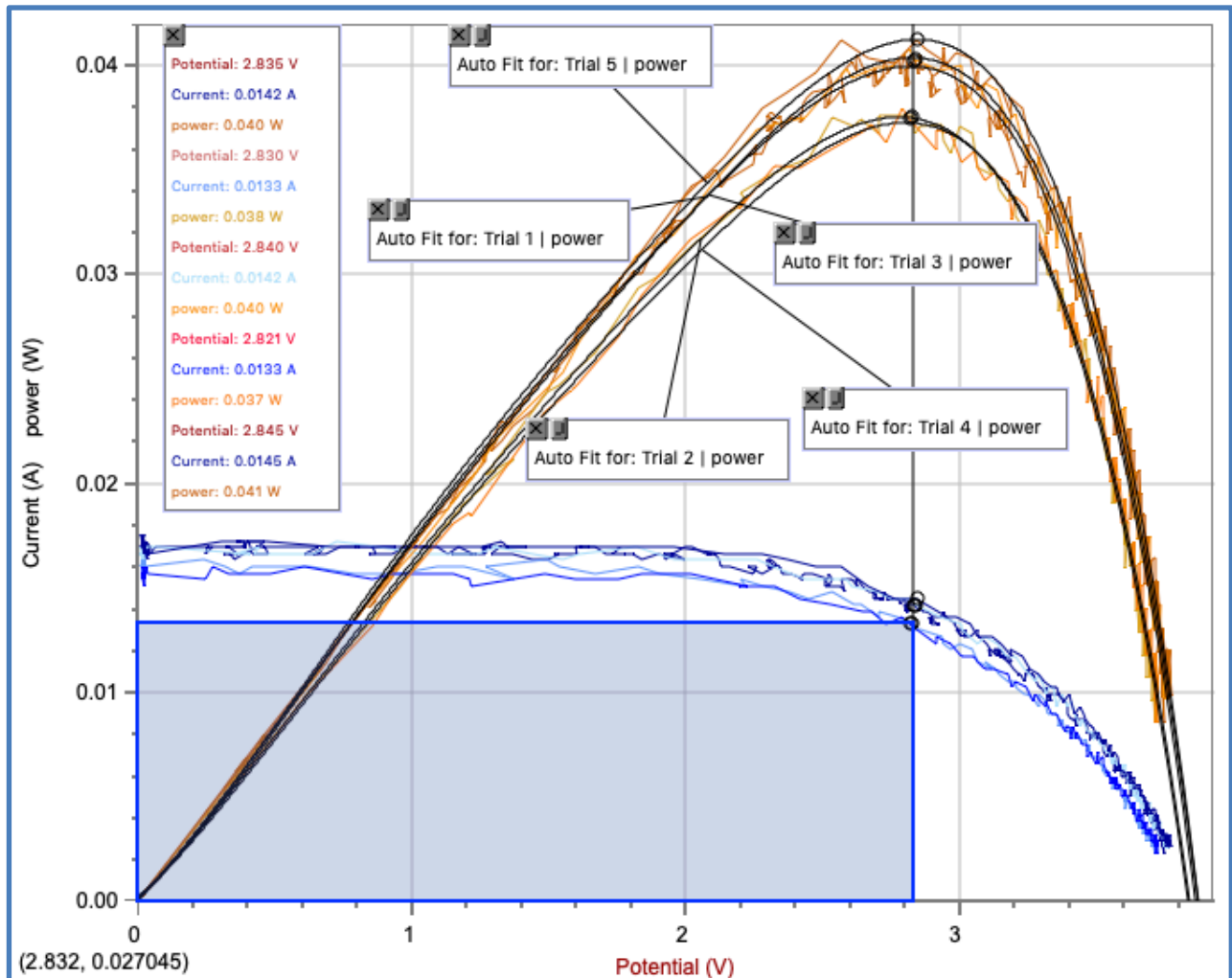


Figure 7. Graph of Current and Power vs. Potential at 420 cm ($G=202 \text{ W} \cdot \text{m}^2$).

As shown in Figure 7 the P-V curve can be plotted on the same set of axes as the I-V graph. A polynomial trendline of degree four or five (depending on which best fit the data) was applied in order to interpolate and smoothen the noisy data. From this, all that remains was to find the polynomial's maximum and record the (P_{MPP}, V_{MPP}) in a spreadsheet for processing. This last step was performed using the Logger Pro inspect tool, displaying the peak coordinates of the polynomial function. Finally, the optimal load resistance $R_{L,MPP}$ could be calculated from current I_{MPP} and voltage V_{MPP} at the timestamp corresponding to the (P_{MPP}, V_{MPP}) pair, as eq. 11, which we know is equal to the internal series resistance R_S [15]:

$$R_L = \frac{V_{MPP}}{I_{MPP}} = R_S \quad (11)$$

Processed data

Table 4: Processed data of IV-curve characteristics at the maximum power point for each distance						
Distance (cm)	Mean Luminosity (Lux)	Mean irradiance ($W \cdot m^{-2}$)	Current (A)	Voltage (V)	Power (W)	External load (Ω)
320	40620	321	0.0234	3.03	0.0707	130
370	30982	245	0.0177	2.89	0.0511	163
420	25546	202	0.0140	2.81	0.0393	202
470	21262	168	0.0116	2.77	0.0322	238
570	14616	115	0.0082	2.56	0.0211	311
620	12756	101	0.0072	2.46	0.0177	344
720	9784	77	0.0055	2.38	0.0131	432
820	7379	58	0.0046	2.24	0.0104	482
920	6199	49	0.0038	2.22	0.0085	585

Analysis

Discussion of data patterns

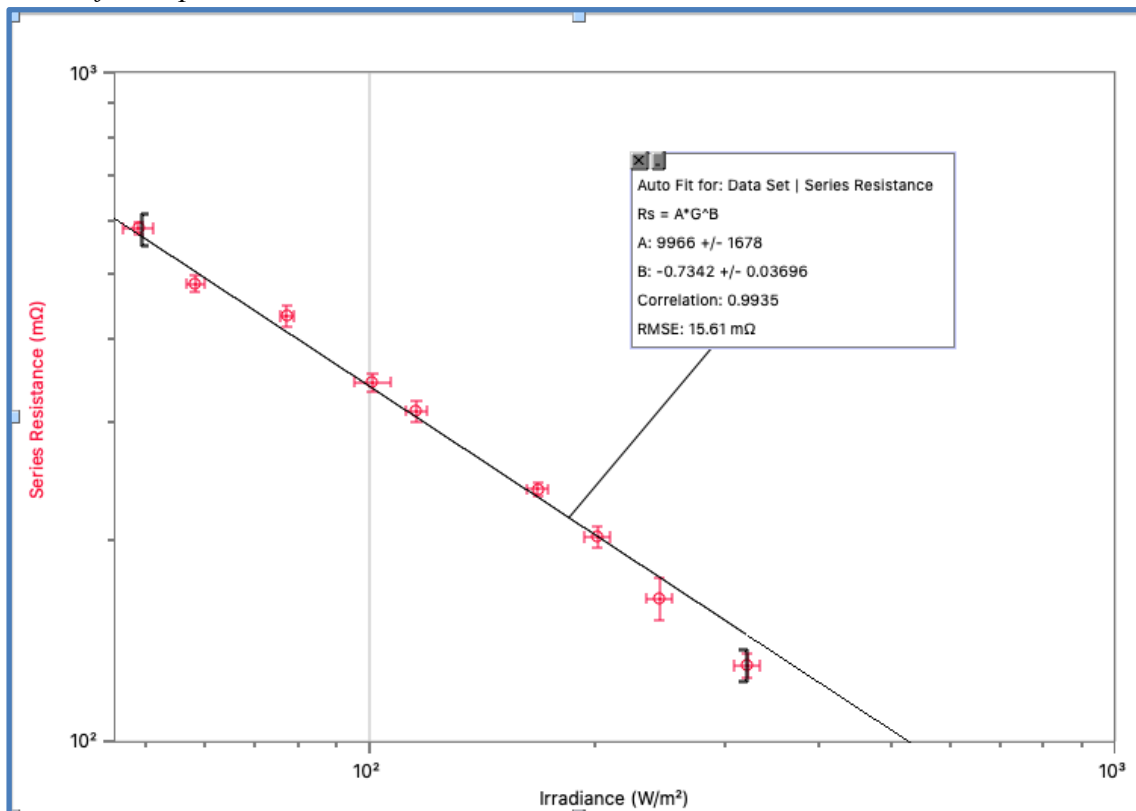


Figure 8. Log-log plot of series resistance (R_S) vs. irradiance (G)

Figure 8 displays a log-log plot of the series resistance plotted against irradiance. The error bars show the mid-range of the 5 trials at each irradiance, as calculated in Table 5 below. A power law regression line trendline for this data was a power relationship of the form $R_S = a \cdot G^b$, where the constants a, b were calculated by the regression model as:

$$a = 9970 \pm 1680$$

$$b = -0.734 \pm 0.0369$$

Interestingly, these values differ considerably from those found by N.H. Reich et al. for their crystalline solar cell, with this investigation's value of a being three times theirs (9970 vs. 3650) and having a larger b exponent value of -0.734 , compared to their -0.975 . The constant b has a percentage uncertainty of 16.9 %, which is quite large, while a has a percentage uncertainty of only 5.0 %--a more acceptable value. It is not clear what exactly causes the variations in these parameters; this would make a good topic for further investigation. A feature of interest is the regression line's very high correlation coefficient (0.9935), which suggests that the implementation of a power law—even if not a valid correlation on a physical level—is highly reliable for this PV cell.

As can be seen in the graph, all nine data points appear to follow the trendline quite closely, with 8 of the 9 points intersecting the trendline with their error bars. However, some deviation is noticeable in the two highest irradiance data points, with the highest reading ($321 \text{ W} \cdot \text{m}^{-2}$) not intersecting the trendline with its error bars at all. There is evidence to suggest that R_S will deviate from the straight line visible in the log-log plot of R_S vs. G at high irradiances [10][16], but these previous studies found that the rate of R_S decrease was lessened—meaning a flattening of the gradient at high G values—as opposed to what could be interpreted as a steepening in the three highest values of our collected data. Given the relatively high uncertainty in a and b , random error may be to blame.

Impact of uncertainties

Statistical trial uncertainty

Uncertainty in the (G, R_S) data points used as error bars in Figure 8 was calculated as the mid-range (MR) of the 5 trials taken per irradiance, as shown in eq. 12, 13:

$$MR(R_S) = \frac{\max(R_S) - \min(R_S)}{2} \quad (12)$$

$$MR(G) = \frac{\max(G) - \min(G)}{2} \quad (13)$$

Producing the following MR absolute uncertainty values for each irradiance-series resistance pair:

Table 5: R_S and G absolute mid-range uncertainties									
Distance (cm)	32	37	42	47	57	62	72	82	92
$MR(R_S)$ (Ω)	13	10	8	6	4	6	2	2	2
$MR(G)$ ($\text{W} \cdot \text{m}^{-2}$)	6	12	8	5	12	11	16	14	12

Apparatus uncertainty

Table 6: Apparatus uncertainty	
Type of apparatus	Uncertainty absolute value
Luxmeter	± 100 lux
Ruler	± 1 cm
Voltmeter	± 0.005 V
Ammeter	± 0.0005 A

Working from the final equation $R_S = a \cdot G^b$:

$$\pm 100 \text{ lux} \approx \pm 0.79 \text{ W} \cdot \text{m}^{-2}$$

Which can be applied to every distance as:

Table 7: Power law uncertainty									
Distance (cm)	32	37	42	47	57	62	72	82	92
Irradiance ($\text{W} \cdot \text{m}^{-2}$)	321	245	202	168	115	101	77	58	49
% Uncertainty lux	0.246	0.323	0.391	0.470	0.684	0.784	1.022	1.355	1.613

Given that power-law coefficient a has % uncertainty of 16.9 % and the power-law exponent b is equal to -0.73 , the overall percentage uncertainty of the outputted R_S prediction is given by eq. 14:

$$\%unc_{R_S} = |(\%unc_{lux} + \%unc_a) \times (b)| \quad (14)$$

Yielding the following overall % uncertainties for each distance:

Table 8: Power law % uncertainty calculations									
Distance (cm)	32	37	42	47	57	62	72	82	92
Irradiance ($\text{W} \cdot \text{m}^{-2}$)	321	245	202	168	115	101	77	58	49
% Uncertainty lux	0.25	0.32	0.39	0.47	0.68	0.78	1.02	1.36	1.61
% Uncertainty a	16.9	16.9	16.9	16.9	16.9	16.9	16.9	16.9	16.9
Value of b	-0.73	-0.73	-0.73	-0.73	-0.73	-0.73	-0.73	-0.73	-0.73
R_S % Uncertainty	12.6	12.6	12.7	12.8	12.9	12.9	13.2	13.4	13.6

With an average % uncertainty in R_S across all trials of ± 12.97 %.

Evaluation

Random errors

P-V graph noise uncertainty

As was visible in Figure 6 and Figure 7, measurements of power were subject to extremely high noise, especially at high voltages (see Figure 9 below). Polynomial regression lines were employed in an attempt to smoothen the data for finding the peak power coordinates, and this was mostly successful.

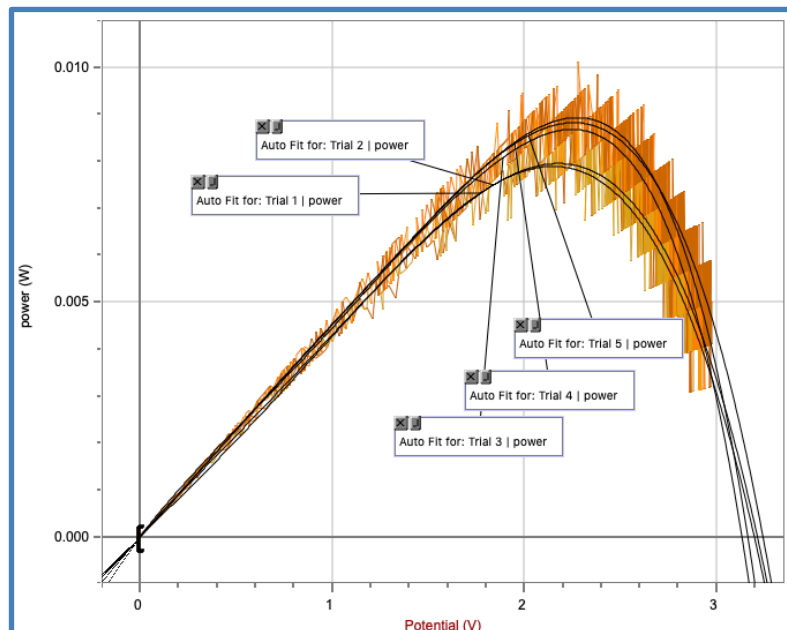


Figure 9. P-V curve with distance 92 cm, showing heavy noise distortion

It appears that the stepped effect between readings (especially evident from 2V onwards) was primarily an issue of the ammeter measuring currents falling within its margin of error. This was likely exacerbated by the cheap potentiometers used in this experiment.

In future trials this could be rectified in several ways: first, by using a more precise ammeter; second, smoothing the noise with a low-pass filter (assuming no significant change in current or voltage); or third, using a computer-controlled cell driver to scan the I-V curve autonomously [17].

Systematic errors

Gauging light intensity

One possible source of error may have been the estimations of the incident irradiance. The luxmeter was only attached to one corner of the panel—which was not necessarily representative of the entire PV-module; this could have perhaps been improved by placing a neutral density filter over the luxmeter. It would have also been preferable to follow the Standard Testing Conditions and use a properly calibrated light source of $1000 \text{ W} \cdot \text{m}^{-2}$ with a solar light spectrum, given that this is the spectrum that the solar panel was designed for. It would also justify the assumption made when converting lux to irradiance: that $G = 0.0079 \cdot \text{lux}$, which is modelled on integrating the solar spectrum specifically [18].

Panel temperature consistency

While no temperature change was discernable to the touch between trials, it is likely that the temperature difference would have had to exceed $\sim 5^\circ\text{C}$ for one to notice, which would translate to a 0.5% efficiency drop per $^\circ\text{C}$ [6]. Therefore, future investigations may benefit from an infrared thermal sensor array pointed at the panel to more reliably determine whether temperature could be skewing the results. It may also be useful to affix the panel to a cooling substrate and/or use a fan to remove excess heat from the panel surface. Alternatively, a copper substrate with an embedded thermocouple could be used for accurate temperature measurements and cooling.

Conclusion

The hypothesis anticipated a power relationship between the internal series resistance and the irradiation incident on the tested solar panel, although no clear estimates could be given for the coefficient or exponent constants, given that these are cell-specific and can only be determined empirically. The findings in this investigation very readily support the existence of a power law, with 8 out of 9 data points intersecting the regression line with their error bars, and a very strong correlation coefficient (0.9935). However, predictions of series resistance in the resultant power-law function have a percentage uncertainty of $\sim 12.97\%$ on average, which indicates that despite a clear power law emerging from the collected data, the exact predictions made using this relationship may be unreliable due to the limitations of the apparatus used.

In future investigations it may be interesting to consider a more detailed model, while reducing the amount of data that needs to be collected such that only key features--such as the x -axis and y -axis intercepts, or 'dark I-V' characteristics--are needed for formulating the constants in the power law. Most importantly, it would be hugely beneficial to compare two or more panels in order to determine the how this relationship changes, and the extent to which it is specific to the solar panels being used.

References

- [1] “Solar Cell Structure | PVEducation.” [Online]. Available: <https://www.pveducation.org/pvcdrom/solar-cell-operation/solar-cell-structure>. [Accessed: 11-Mar-2020].
- [2] “MPP Tracking | EME 812: Utility Solar Power and Concentration,” *Penn State Department of Energy and Mineral Engineering*. [Online]. Available: <https://www.e-education.psu.edu/eme812/node/713>. [Accessed: 10-Mar-2020].
- [3] M. Turek, “Current and illumination dependent series resistance of solar cells,” *J. Appl. Phys.*, vol. 115, no. 14, p. 144503, Apr. 2014, doi: 10.1063/1.4871017.
- [4] E. Saloux, A. Teysedou, and M. Sorin, “Explicit model of photovoltaic panels to determine voltages and currents at the maximum power point,” *Sol. Energy*, vol. 85, no. 5, pp. 713–722, May 2011, doi: 10.1016/j.solener.2010.12.022.
- [5] W. Shinong, M. Qianlong, X. Jie, G. Yuan, and L. Shilin, “An improved mathematical model of photovoltaic cells based on datasheet information,” *Sol. Energy*, vol. 199, pp. 437–446, Mar. 2020, doi: 10.1016/j.solener.2020.02.046.
- [6] E. Cuce, P. M. Cuce, and T. Bali, “An experimental analysis of illumination intensity and temperature dependency of photovoltaic cell parameters,” *Appl. Energy*, vol. 111, pp. 374–382, Nov. 2013, doi: 10.1016/j.apenergy.2013.05.025.
- [7] “Maximum Power Transfer Theorem (MPTT) | Proof, Example,” *Electronics Hub*, 04-Jun-2019. [Online]. Available: <https://www.electronicshub.org/maximum-power-transfer-theorem/>. [Accessed: 12-Mar-2020].
- [8] M. Chegaar, A. Hamzaoui, A. Namoda, P. Petit, M. Aillerie, and A. Herguth, “Effect of Illumination Intensity on Solar Cells Parameters,” *Energy Procedia*, vol. 36, pp. 722–729, Jan. 2013, doi: 10.1016/j.egypro.2013.07.084.
- [9] Priyanka, M. Lal, and S. N. Singh, “A new method of determination of series and shunt resistances of silicon solar cells,” *Sol. Energy Mater. Sol. Cells*, vol. 91, no. 2, pp. 137–142, Jan. 2007, doi: 10.1016/j.solmat.2006.07.008.
- [10] M. D. Lammert and R. J. Schwartz, “The interdigitated back contact solar cell: A silicon solar cell for use in concentrated sunlight,” *IEEE Trans. Electron Devices*, 1977, doi: 10.1109/T-ED.1977.18738.
- [11] F. Khan, S. N. Singh, and M. Husain, “Effect of illumination intensity on cell parameters of a silicon solar cell,” *Sol. Energy Mater. Sol. Cells*, vol. 94, no. 9, pp. 1473–1476, Sep. 2010, doi: 10.1016/j.solmat.2010.03.018.
- [12] N. H. Reich *et al.*, “Crystalline silicon cell performance at low light intensities,” *Sol. Energy Mater. Sol. Cells*, vol. 93, no. 9, pp. 1471–1481, Sep. 2009, doi: 10.1016/j.solmat.2009.03.018.
- [13] P. Kärhä, M. Ojanen, S. Nevas, A. Sperling, and E. Ikonen, “Tungsten Filament Lamps as Absolute Radiometric Reference Sources,” p. 13, 2011.
- [14] “Amazon.com: OSRAM FCS 64640 150W 24V HLX Halogen Light Bulb: Home Improvement.” [Online]. Available: <https://www.amazon.com/OSRAM-64640-150W-Halogen-Light/dp/B000QHADQI>. [Accessed: 10-Mar-2020].
- [15] H. Ibrahim and N. Anani, “Variations of PV module parameters with irradiance and temperature,” *Energy Procedia*, vol. 134, pp. 276–285, Oct. 2017, doi: 10.1016/j.egypro.2017.09.617.
- [16] M. Wolf and H. Rauschenbach, “Series resistance effects on solar cell measurements,” *Adv. Energy Convers.*, vol. 3, no. 2, pp. 455–479, Apr. 1963, doi: 10.1016/0365-1789(63)90063-8.

- [17] S. K. Datta, K. Mukhopadhyay, S. Bandopadhyay, and H. Saha, "An improved technique for the determination of solar cell parameters," *Solid-State Electron.*, vol. 35, no. 11, pp. 1667–1673, Nov. 1992, doi: 10.1016/0038-1101(92)90196-J.
- [18] "Howto convert solar intensity in LUX to watt per meter square for sunlight?," *ResearchGate*. [Online]. Available: https://www.researchgate.net/post/Howto_convert_solar_intensity_in_LUX_to_watt_per_meter_square_for_sunlight. [Accessed: 12-Mar-2020].

Appendix

Table 9: Full data of IV-curve characteristics at the maximum power point							
Distance (cm)	Trial Number	Mean Luminosity (Lux)	Mean irradiance (W/m ²)	At the MPP:			
				Current	Voltage	Power	External load
32	1	38940	308	0.0225	2.99	0.0671	133
32	2	41890	331	0.0237	3.09	0.0731	131
32	3	38850	307	0.0224	3.01	0.0673	134
32	4	41400	327	0.0238	3.01	0.0716	127
32	5	42020	332	0.0246	3.03	0.0746	123
37	1	31870	252	0.0182	2.95	0.0536	162
37	2	30890	244	0.0179	2.95	0.0528	165
37	3	30680	242	0.0172	2.91	0.0502	169
37	4	29480	233	0.0169	2.90	0.0489	172
37	5	31990	253	0.0183	2.72	0.0499	148
42	1	25950	205	0.0142	2.82	0.0399	199
42	2	24670	195	0.0135	2.78	0.0376	205
42	3	26010	205	0.0143	2.83	0.0404	198
42	4	24520	194	0.0133	2.81	0.0373	211
42	5	26580	210	0.0145	2.84	0.0413	196
47	1	21870	173	0.0118	2.81	0.0330	239
47	2	21660	171	0.0117	2.77	0.0323	238
47	3	20450	162	0.0116	2.71	0.0315	233
47	4	21640	171	0.0120	2.84	0.0339	237
47	5	20690	163	0.0111	2.71	0.0301	243
57	1	14280	113	0.0081	2.52	0.0204	311
57	2	14610	115	0.0082	2.52	0.0208	305
57	3	15150	120	0.0086	2.59	0.0222	302
57	4	14840	117	0.0082	2.59	0.0213	314
57	5	14200	112	0.0080	2.60	0.0207	325
62	1	13360	106	0.0075	2.54	0.0191	336
62	2	12580	99	0.0074	2.46	0.0183	331
62	3	12690	100	0.0072	2.47	0.0177	345
62	4	11950	94	0.0069	2.44	0.0169	353
62	5	13200	104	0.0068	2.42	0.0165	353
72	1	9876	78	0.0055	2.44	0.0135	440
72	2	9741	77	0.0054	2.38	0.0129	437
72	3	9561	76	0.0056	2.31	0.0130	410
72	4	9777	77	0.0054	2.41	0.0131	443
72	5	9964	79	0.0055	2.38	0.0131	431
82	1	7603	60	0.0045	2.24	0.0101	497
82	2	7439	59	0.0047	2.20	0.0104	469
82	3	7277	57	0.0047	2.27	0.0107	480
82	4	7197	57	0.0046	2.23	0.0103	482
82	5	7381	58	0.0047	2.25	0.0105	484
92	1	6308	50	0.0037	2.15	0.0079	586
92	2	5798	46	0.0036	2.18	0.0080	599
92	3	6202	49	0.0039	2.25	0.0087	582
92	4	6308	50	0.0039	2.28	0.0089	581
92	5	6378	50	0.0039	2.25	0.0088	575